Elevated Post K-Pg Export Productivity in the Gulf of Mexico and Caribbean

Christopher M. Lowery[1]*, Timothy J. Bralower[2]

[1]University of Texas Institute for Geophysics, Austin, TX

[2]Pennsylvania State University, University Park, PA

*corresponding author: cmlowery@utexas.edu

Abstract

The global heterogeneity in export productivity after the Cretaceous-Paleogene (K-Pg) mass extinction is well documented, with some sites showing no change on geologic timescales, some demonstrating sustained decline, and a few showing a somewhat surprising increase. However, these records come from sites so widespread that a key outstanding question is the geographic scale of changes in export productivity, and whether similar environments (open ocean gyres, western boundary currents) responded similarly or whether heterogeneity is unrelated to environment. To address this, we developed three new Ba/Ti export productivity records from sites in the Gulf of Mexico and Caribbean which, combined with published data from a fourth site in the Chicxulub Crater itself, allows us to reconstruct regional changes in post K-Pg export productivity for the first time. We find that, on a regional scale, export productivity change is homogenous, with all four sites showing a ~300 kyr period of elevated export production just after the boundary, followed by a longer period of decline. Interestingly, this interval of elevated export production appears to coincide with the post K-Pg global micrite layer, which is thought to at least partially have been produced by blooms of carbonate-producing cyanobacteria and other picophytoplankton. We note from a global comparison of sites that elevated export productivity appears to be most common in tropical waters, which suggests that changing plankton ecology evidenced

by the micrite layer altered the biological pump in a way that encouraged a temporary increase in export production in the tropics.

Plain Language Summary

Primary producers are the base of the food chain, and this group was severely damaged by the environmental effects associated with the end Cretaceous mass extinction. Understanding how primary production recovered after this calamity is thus an important foundation for understanding how ecosystems recovered. Most previous work on this topic has focused on a process called export production, whereby primary production is transferred to the seafloor (and preserved in the geologic record). This work has shown that although most parts of the ocean recorded a decline in export production after the extinction event, some regions actually showed an increase. However, it was not clear on what scale these differences occurred, or what caused them. Here, we generated three new records of export production from a single region, the Gulf of Mexico/Caribbean Sea, and found a consistent increase in export production at each site for the same period of time after the extinction event. Comparison with other sites with increased export production shows that many are from low latitudes and suggests that these regions were predisposed to increased export production in the earliest Paleocene.

1. Introduction

The end Cretaceous mass extinction is associated with a severe disruption of marine productivity (Hsu and Mackenzie, 1985; Zachos et al., 1989; D'Hondt et al., 1998; Coxall et al., 2003; Birch et al., 2016). A reduction in sunlight caused by dust, soot, and sulfate aerosols ejected by the Chicxulub impact resulted in a reduction in photosynthesis which is believed to have led to the collapse of marine food webs (Alvarez et al., 1980; D'Hondt et al 1998). Models show that the reduction in insolation lasted only a few years after the impact (Toon et al., 1997; Bardeen et al., 2016; Brugger et al., 2016; Artemieva et al., 2016; Artemieva and Morgan, 2020), removing the proximal external stress on marine primary producers and clearing the way for their recovery. How, exactly, marine productivity recovered has been a central

focus of K-Pg boundary research for decades; the K-Pg mass extinction represents a geologically unique disruption of marine ecosystems, perhaps the only major event in Earth history which happened faster than modern climate change and environmental disruption. Modern oceans are likely on the verge of a major reorganization of dominant plankton types due to warming, acidification, and changes in circulation patterns (e.g., Barton et al., 2016; Jonkers et al., 2019), and primary production is expected to decline 20% due to warming (Moore et al., 2018). The earliest Paleocene provides a window into understanding how such ecological changes may impact food webs and marine carbon burial.

Of course, we can't observe ancient primary production in the euphotic zone directly, and so most work on the collapse and recovery of productivity after the K-Pg boundary is focused on sedimentary records of export production (the transfer of organic matter from the euphotic zone to the deep sea; Zhang et al., 2018). The downward movement of organic matter is accomplished by a mechanism called the "biological pump," whereby organic matter is moved via biological pathways like fecal pellets or marine snow, the daily vertical migration of plankton, the sinking of particulate organic matter, etc. (Zhang et al., 2018). The functioning of the pump is controlled both by the amount of net primary production that is exported from the euphotic zone (~100 m water depth), where it can no longer be instantly reused in new primary production, and the amount of that organic matter which survives grazing at intermediate depths to reach the depth where it has been effectively removed from the short-term carbon cycle (commonly considered to be > 1000 m) (Boyd and Newton, 1995; Buessler, 1998; Legendre and Rivkin, 2002; Boyd and Trull, 2007; Buessler and Boyd, 2009; Henson et al., 2012). The amount of net primary production that reaches the deep sea varies by region and is largely controlled by plankton ecology (Henson et al., 2012), but on the whole only 1-3% of modern net primary production reaches the deep sea (e.g., Müller and Suess, 1979; de la Rocha and Passow, 2007).

Initial reconstructions of productivity change across the K-Pg boundary focused on carbonate proxies, specifically carbonate mass accumulation rates and carbon stable isotopes (e.g., Hsü and Mackenzie, 1985; Zachos et al., 1989) A drop in carbonate mass accumulation rate in the deep sea has

been observed at many boundary sites across the globe, and is interpreted to represent a reduction in the production of carbonate by pelagic calcifiers like calcareous nannoplankton and planktic foraminifera (e.g., D'Hondt et al., 1998), both of which suffered a severe (>90% species diversity) extinction at the K-Pg boundary (e.g., Thierstein, 1982; Bown, 2005; Fraass et al., 2015; Lowery et al., 2020). The most striking carbonate proxy response, though, is the collapse of the $\delta^{13}C$ gradient between the surface ocean and the deep sea (Zachos and Arthur, 1986; Zachos et al., 1989; D'Hondt et al., 1998; Coxall et al., 2003; Esmeray-Senlet, 2015; Birch et al., 2016). In the modern ocean (and through most of the last 150 myr, at least) the sinking of ^{12}C-rich organic matter depletes the surface ocean of that light isotope and enriches the seafloor in it, resulting in an isotopic gradient from surface to seafloor. This gradient collapsed at the Cretaceous-Paleogene (K-Pg) boundary, reflecting a reduction in export production and a weakening of the biological pump for 1.8 myr (e.g., Kump, 1991; Birch et al., 2016, 2021). Modelling suggests that a ~50% decrease in the amount of organic carbon exported from the surface ocean, from 10% of net primary production to 5%, would account for the observed collapse of the $\delta^{13}C$ gradient (D'Hondt et al., 1998; Henehan et al., 2019).

The continued flux of some organic matter to the deep sea is confirmed by geochemical data which indicate a rapid recovery of primary producers (Sepúlveda et al., 2009, 2019) and fossil data which indicate a lack of extinction in pelagic fishes (Doyle, 1979; Siebert and Norris, 2015) and deep sea benthic foraminifera (e.g., Culver, 2003; Alegret and Thomas, 2005, 2007, 2009; Alegret et al., 2012). One of the most striking features of the benthic foraminiferal record at the K-Pg boundary is how it varies globally. Although no major extinction occurred, assemblages shifted at many sites (e.g., Culver et al., 2003). At some localities, benthic foraminifer assemblages indicate a reduction in the flux of organic matter to the seafloor, but others show no change across the boundary, and some actually indicate an *increase* in organic matter flux (e.g., Alegret and Thomas 2005, 2007, 2009).

This heterogeneity reveals a weakness in the use of carbon isotope gradients to reconstruct post K-Pg export production. Isotopic analysis of planktic and benthic foraminifera requires well-preserved

carbonate material, otherwise diagenetic overprinting will obscure the signal. Localities with well-preserved 66-myr-old foraminifera are not particularly common, and for that reason carbon isotope gradients have only been produced from a handful of well-studied sites like Walvis Ridge (Hsu and Mackenzie, 1985; D'Hondt, 1998a; Coxall et al., 2006; Birch et al., 2016, 2021), Shatsky Rise (Zachos and Arthur, 1986; Zachos et al., 1989; Coxall et al., 2006), J-Anomaly Ridge (Zachos and Arthur, 1986), and Sao Paolo Plateau (Zachos and Arthur, 1986). While these sites have all yielded high quality data that have fundamentally changed our understanding of K-Pg recovery, they only cover a small part of the ocean.

For this reason, additional proxies not dependent on pristine microfossil preservation are necessary. Benthic foraminifera are one such proxy, and another is based on barium. Biogenic barium (commonly preserved as barite – $BaSO_4$) abundance in marine sediments has been shown to correlate with export production in the modern and ancient ocean (Dymond et al., 1992; Francois et al., 1995; Eagle et al., 2003; Paytan and Griffith, 2007) and is not subject to the same diagenetic effects as carbon isotopes. When applied to ancient sediments, this paleoproductivity proxy is commonly normalized against a terrigenous element like titanium or aluminum to control for any possible detrital barium component (e.g., Dymond et al., 1992; Payton et al., 1996; Bains et al., 2000; Paytan and Griffith, 2007; Griffith and Paytan, 2012). Hull and Norris (2011) used Ba/Ti and Ba/Fe ratios from a number of K-Pg boundary sites to bolster the export productivity record of benthic foraminifera, and demonstrated that changes in export production across the boundary were indeed geographically heterogeneous, with some sites showing an increase in export production after the boundary.

Understanding geographic heterogeneity in export production is necessary to understand the overall recovery of marine primary producers after the K-Pg boundary. In particular, the calcareous nannoplankton, which have the best fossil record among primary producers in the early Paleocene, exhibit geographic heterogeneity in their post K-Pg recovery (Jiang et al., 2010; Schueth et al. 2015; Jones et al., 2019). Post-extinction calcareous nannoplankton assemblages are characterized by a dominance of

"disaster taxa," chiefly *Braarudosphaera* and *Cervisiella,* which eventually give way to a succession of acme events as new Paleocene genera appear and briefly dominate the assemblage (Bown, 2005; Jones et al., 2019; Gibbs et al., 2020). The timing of this transition is geographically variable, and at sites with elevated export productivity after the K-Pg (Shatsky Rise and Chicxulub Crater), it is coincident with an observed decline in export production (Jones et al., 2019). In the ocean today, eutrophic waters tend to be dominated by a few taxa best suited to take advantage of widely available food, while oligotrophic waters tend to have much higher diversity with greater degrees of specialization (e.g., Hallock, 1987). Jones et al. (2019) hypothesize that the recovery of primary producer assemblages after the K-Pg is similarly linked to nutrient state controlled by the recovery of the biological pump, but the linkages are not well understood and a better picture of export productivity trends is a necessary first step.

Unfortunately, the geographic trends in early Paleocene export productivity are still poorly known. Although the work of Hull and Norris (2011) represents a significant improvement in understanding these trends, it is still limited to the ocean basin scale: Shatsky Rise in the equatorial Pacific compared to Walvis Ridge in the South Atlantic compared to Maud Rise in the Southern Ocean. This is a good starting place but leaves open the question of the scale of heterogeneity. Do regions exhibit similar trends (perhaps implying an oceanographic driver of variability) or do sites vary even within a region (perhaps implying that variability is driven by local effects or is just stochastic)? To address this question, we developed three new Ba/Ti datasets from the Gulf of Mexico and Caribbean at Deep Sea Drilling Project (DSDP) Site 95 and Ocean Drilling Program (ODP) Sites 999 and 1001, which we combined with published data from International Ocean Discovery Program (IODP) Site M0077 in the Chicxulub Crater (Lowery et al., 2021) to produce the first regional-scale study (~1700 km) of export productivity after the K-Pg. We found that earliest Danian export productivity is elevated at all Gulf of Mexico and Caribbean sites and that an initial reduction in export production occurs ~ 300 kyr after the boundary at all sites, indicating that export productivity trends are homogeneous at a regional scale.

1.1 Study Sites

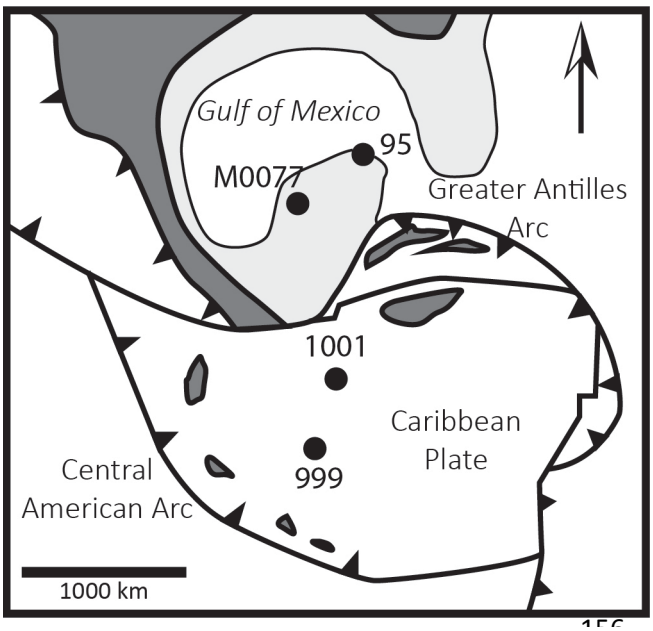

Figure 1. *Map showing position of our study sites around the time of the K-Pg Boundary. Map modified after Pindell and Barrett (1990) and Snedden et al. (2021).*

We looked at three scientific ocean drilling sites in the greater Caribbean region with an identified and well-preserved K-Pg boundary interval (Figure 1). These tropical/subtropical sites are characterized by pelagic carbonate deposition throughout the study interval and, given their oceanographic setting and dominant sediment type, were likely generally oligotrophic from the Cretaceous into the Paleogene. An additional site, DSDP Site 536, below the Campeche Escarpment in the southeastern Gulf of Mexico (Buffler et al., 1984), was considered but rejected because a preliminary examination of planktic foraminifera in the nominally lowermost Paleocene cores found a mix of biozones ranging from the Cretaceous to the late Paleocene, indicating significant bioturbation and/or drilling disturbance, suggesting that XRF data would be untrustworthy. Nearby DSDP Site 95, drilled in 1970 on the northeasterly margin of the Yucatan Platform on a feature called the Campeche Escarpment (Worzel et al., 1973), contained the correct order of planktic foraminifer biozones and decent preservation in a mostly-complete section overlying the K-Pg impact layer. The Chicxulub impact (and associated earthquakes, tsunami, and seiche waves) caused widespread mass-wasting across the Gulf of Mexico, resulting in K-Pg boundary deposits 10s to 100s of m thick (e.g., Bralower et al., 1998; Denne et al., 2013; Sanford et al., 2016). Site 95, due to its perched position on the edge of the Yucatan Platform, only has ~ 3 m of reworked Cretaceous material and impact debris (Figure 2A). The top of the K-Pg boundary layer occurs at the top of Core 13. This is not the K-Pg boundary per se, because the base of the Paleocene is defined at its Global Stratotype Section and Point at El Kef, Tunisia, as the lowest occurrence of impact material; in other words, the Cretaceous ended at "the

moment of the meteorite impact" (Molina et al., 2009). The impact layer in the Gulf of Mexico is thus technically earliest Danian in age.

Two ODP sites in the Caribbean Sea contain well-constrained K-Pg boundary intervals. Site 1001 was drilled in 1997 during Leg 165, and is located on a feature called the Hess Escarpment on the Nicaragua Rise (Figure 1). Shipboard biostratigraphy placed the K-Pg boundary between Core 1001A-38R-CC (Figure 2B). Unlike the thick K-Pg boundary deposits found in the Gulf of Mexico, here the

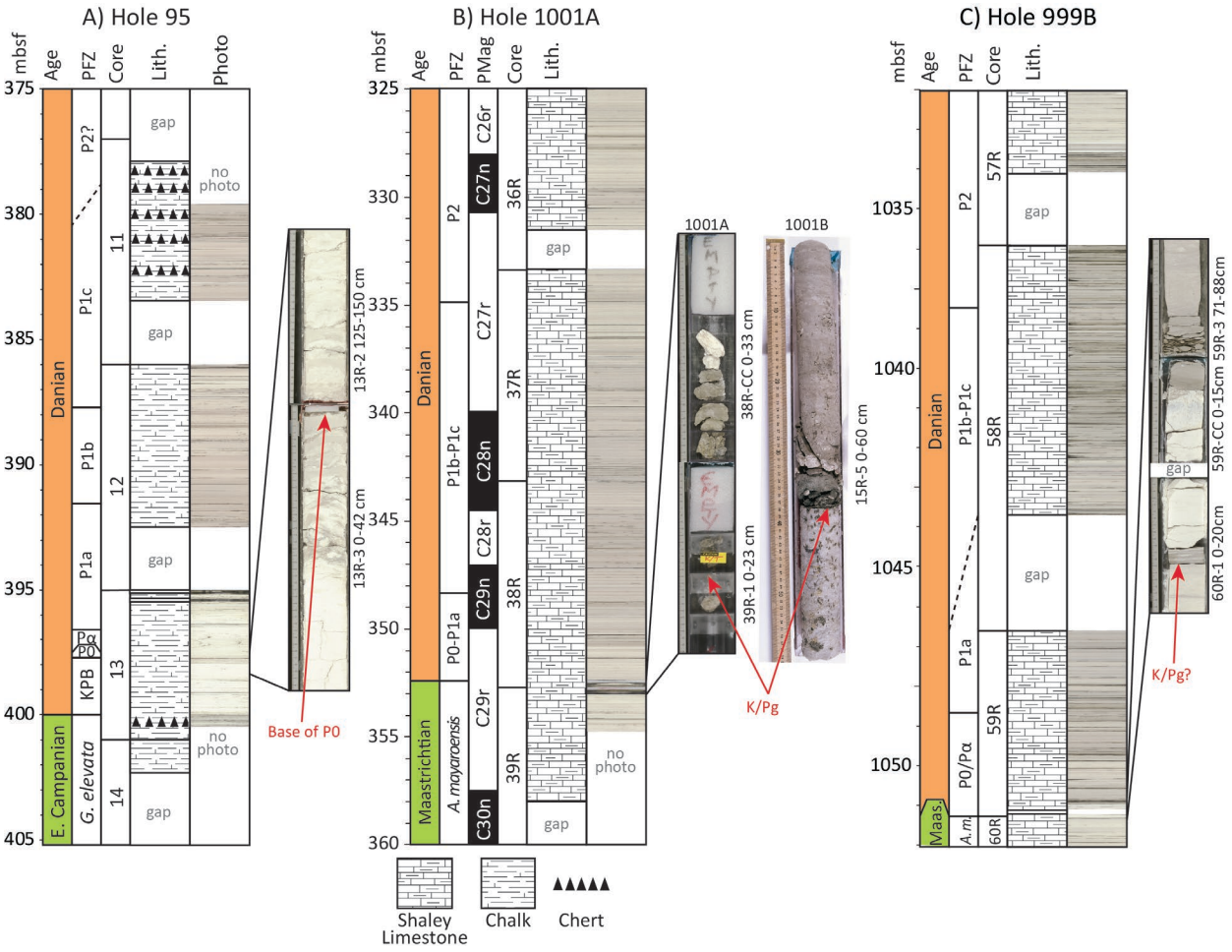

Figure 2. *Stratigraphic sections showing lithostratigraphy, core scan photographs, and images of the K-Pg boundary of the studied intervals from DSDP Hole 95, ODP Hole 1001A, and ODP Hole 999B. Lithostratigraphy follows shipboard descriptions Worzel, Bryant et al. (1973) for Site 95 and Sigurdsson et al., 1997 for Sites 999 and 1001). Core scan photographs were collected at the GCR at the same time XRF data were collected (except for the photograph of the K-Pg boundary in Hole 1001B, which is from the ODP photo archives). Mbsf = meters below sea floor, PFZ = Planktic Foraminifer Zone, Lith. = lithology, PMag = Paleomagnetic polarity, E. Campanian = Early Campanian, Maas. = Maastrichtian, G. elevata = Globotruncanita elevata, A.m. and A. mayaroensis = Abathomphalus mayaroensis.*

whole interval is just a few cm thick. Maastrichtian limestone is overlain by a 1 cm thick dark greenish gray clay, which is in turn overlain by a 3.5 cm bluish gray claystone containing 1 mm scale dark green spheroids interpreted to be tektites (Sigurdsson et al., 1997). This tektite layer is turn overlain by 3.5 cm medium gray to greenish gray claystone which contains shocked quartz (Sigurdsson et al., 1997). The boundary sequence is overlain by a 4 cm thick light grey limestone assigned to planktic foraminifer biozones P0/Pα undifferentiated based on thin section analysis (the zones are undifferentiated because the biostratigraphers were not confident in their ability to identify the taxon differentiating the zones, *P. eugubina*, in thin section; Sigurdsson et al., 1997). Shipboard biostratigraphy in the Paleocene is of poor quality due to the extremely poor preservation of fossil material in the indurated limestone. Fortunately, magnetic polarity was published for Site 1001 by Louvel and Galbrun (2001) based on whole core scans and single samples, as well as a downhole wireline tool called the Geological High-sensitivity Magnetic Tool (GHMT), and the resulting magnetic reversal timescale means that Site 1001 has the best age model of the sites examined here. Although Hole 1001B recovered a more complete boundary section than Hole 1001A (Figure 2B), Hole 1001B has a number of coring gaps in both the latest Cretaceous and the early Paleocene, so XRF scans were conducted on Hole 1001A.

Site 999 was also drilled in 1997 during Leg 165 and is located on a small feature called Kogi Rise in the Colombian Basin (Figure 1). Shipboard biostratigraphy placed the K-Pg boundary near the boundary between Cores 59 and 60 (Figure 2C). The highest occurrence of common Maastrichtian calcareous nannoplankton was observed in Sample 999B-60R-1 10 cm, and that of Maastrichtian planktic foraminifera in a thin section in Sample 999B-60R-1 1-21 cm (Sigurdsson et al., 1997). The few foraminifera were observed in thin section between Samples 999B-59R-CC 15cm (the base of the core catcher) and 999B-60R-1 1 cm were composed primarily of survivor species *Guembelitria cretacea* (Sigurdsson et al., 1997). The shipboard biostratigraphers were not confident that tiny trochospiral specimens observed in the same sample were or were not *Parvularugoglobigerina eugubina* (the marker taxon for the base of planktic foraminifer zone Pα) and thus conservatively assigned this interval to zones

P0/Pα undifferentiated (Sigurdsson et al., 1997). The bases of zones P1a (top of *P. eugubina*), P1b (base of *Subbotina triloculinoides*), and P2 (base of *Praemurica uncinata*) were identified shipboard (Sigurdsson et al., 1997) and form the basis for the age model used here, although the latter two are of lower confidence. We washed and examined samples from Site 999 to see if we could refine the shipboard age model but poor microfossil preservation in the indurated limestone material prevented us from adding anything new. A white indurated limestone overlies the highest Cretaceous nannoplankton observed in Core 60, and the base of Section 59R-CC contains a 1 mm thick claystone. Comparison of the recovered core and borehole images collected by the formation microscanner tool reveals that this claystone is ~ 9 cm thick in the borehole, and thus ~ 8 cm of this unit were not recovered (Sigurdsson et al., 1997). It seems reasonable to assume that this missing interval is equivalent to the 8 cm of ejecta-bearing claystones described at Site 1001. The claystone is overlain by 10 cm thick mottled blue limestone described by shipboard scientists as having the appearance of "Roquefort Blue Cheese" and assigned to planktic foraminifer zones P0/Pα (Sigurdsson et al., 1997). This white limestone is a common feature of K-Pg boundary sections in the deep sea, and is comprised of micrite (i.e., microcrystalline calcite) that is thought to have multiple possible origins including: (1) production by blooms of calcifying picoplankton like cyanobacteria in surface-ocean "whiting" events in the aftermath of the extinction of larger primary producers, and (2) backreaction of CaO and CaOH produced during the impact (Bralower et al., 2020). Although the white limestone only extends 10 cm above the boundary, Bralower et al. (2020) observed micrite at Site 999 over a total thickness of 2.42 m. A 2 m coring gap occurs at the base of Core 58 in planktic foraminifer Zone P1a. Micrite was also identified at Site 1001 but it was limited to the core catcher of core 1001A-38R, which contains a few discontinuous bits if rubble and a large void space (Figure 2B), so Bralower et al. (2020) considered the observed 17 cm interval to be a minimum.

2. Methods

We scanned the cores at the XRF Core Scanning Lab at the IODP Gulf Coast Repository at Texas A&M University in College Station, TX. The archive halves of selected cores were scraped to ensure a

fresh face of the core for scanning, and, in the case of the softer sediments of Site 95, to ensure a flat surface for the XRF core scanner. Lithified sections from Site 999 and 1001 were likewise scraped and leveled within the core liner to ensure a flat surface. Cores were then covered with 4 μm thick Ultralene film to prevent sediment from sticking to the scanner.

Cores were scanned on an Avaatech XRF Core Scanner at two excitation conditions focused on different element groups. The first scan was at 10kVp with no filter to analyze major and minor elements (Al, Si, K, Ca, Ti, Mn, Fe, Cr, P, S, and Mg) and the second was at 50kVp with a Cu filter to analyze heavier trace elements (Sr, Rb, Zr, and Ba). Scan resolution was set depending on relative distance above the K-Pg boundary, based on low resolution shipboard biostratigraphy. Core sections within zone Pα or the lower part of zone P1a (very roughly, within ~ 500 kyr of the boundary) were scanned at 1 or 2 cm steps, and sections deposited below the boundary and >500 kyr after the boundary were scanned at 5 cm steps. Some steps were skipped or moved based on visual examination of the core before scanning (e.g., to avoid cracks or uneven surfaces). Laboratory standards were run at the beginning and end of each day to monitor instrumental performance.

Raw spectrum data were processed into peak areas in the lab using the software program bAxil. Quality control of processed data was carried out using the following parameters: 1) throughput (samples with values <150,000, which indicates a gap between the sensor and the core, were removed); 2) Argon peak (samples with positive values, indicating that the sensor was measuring ambient air, were removed); and 3) standard deviation (samples with elemental peaks of Ba or Ti within 2 standard deviations of zero were removed).

To improve the age model for this study we analyzed planktic foraminifera from Site 95 at a resolution of up to 5 cm. Lightly lithified samples were gently broken into cm-sized chunks using a mortar and pestle. All samples were soaked in a solution of hydrogen peroxide and borax for at least 48 hours and then washed over a 45 μm sieve to ensure capture of typically very small early Paleocene taxa; the sieve was soaked in methylene blue dye between samples to mark contaminants. Finally, samples

were dried overnight in an oven. Samples were examined for presence/absence of key marker species on a Zeiss Discovery.V8 light microscope. Species concepts follow those of Olsson et al., (1999); biozones are the Wade et al. (2011) update of the Paleocene biozonation scheme published by Berggren and Pearson (2005). Dates reported are those found in Gradstein et al. (2012).

Sites 999 and 1001 are lithified and characterized by very poor fossil preservation in some pilot samples we examined, and so we did not attempt detailed biostratigraphic analysis on either site. Therefore the age model for both cores reflects shipboard biostratigraphy (Sigurdsson et al., 1997) and published paleomagnetic data for Site 1001 (Louvel and Galbrun, 2001).

3. Results

3.1 Biostratigraphy

Site 95 is comprised of firm but unlithified calcareous ooze that yielded fairly well preserved material. We examined 25 samples from Cores 11 to 13 to identify and then refine the boundaries between planktic foraminifer biozones. An obvious lithologic change occurs in Section 95-13R-3 at 24 cm. Samples below this level are composed of mixed Cretaceous species remobilized by impact-induced seismic disturbance and tsunami, termed the K-Pg Boundary Cocktail (Bralower et al., 1998). From Sample 95-13R-2, 139 cm to Sample 95-13R-3, 24 cm, the core is mottled and contains some signs of drilling disturbance (biscuiting, soft sediment deformation). Samples taken within what we interpret to be the biscuits, however, contain mostly Cretaceous species until 95-13R-3, 0-2 cm, where the survivor species *Guembelitria cretacea* starts to become more common; this level is assigned to the base of zone P0. The base of zone Pα, based on the lowest occurrence of *P. eugubina,* is found just above this level, between 130 and 140 cm in Section 95-13R-2. The base of overlying zone P1a, based on the highest occurrence of *P. eugubina*, occurs between 130 and 140 cm in Section 95-13R-1. Most of zone P1a is erased by a coring gap, but zone Pα and the portion of zone P1a preserved here contain abundant calcispheres, the resting cyst of calcareous dinoflagellates. Above the coring gap between Cores 95-12R

and 13R, the bases of zone P1b (lowest occurrence of *S. triloculinoides*) and zone P1c (lowest occurrence of *Globanomalina compressa*) are both present. The base of zone P2 (*P. uncinata*) is missing in another coring gap between Cores 11R and 12R, and the age model from the base of zone P1c to the coring gap is based on extrapolating the sedimentation rate from zone P1b; this method suggests that most of zone P1c is present.

3.2 Ba/Ti

3.2.1 Site M0077

Data from the Chicxulub Crater have been published previously (Lowery et al., 2018, 2021) but contain several interesting trends that should be summarized here. The highest Ba/Ti ratios in the study interval are found in the earliest Paleocene, covering the first ~320 kyr after the impact (Figure 3A). At that point, there is a sharp drop in Ba/Ti values, followed by a steady decline from moderate values to a

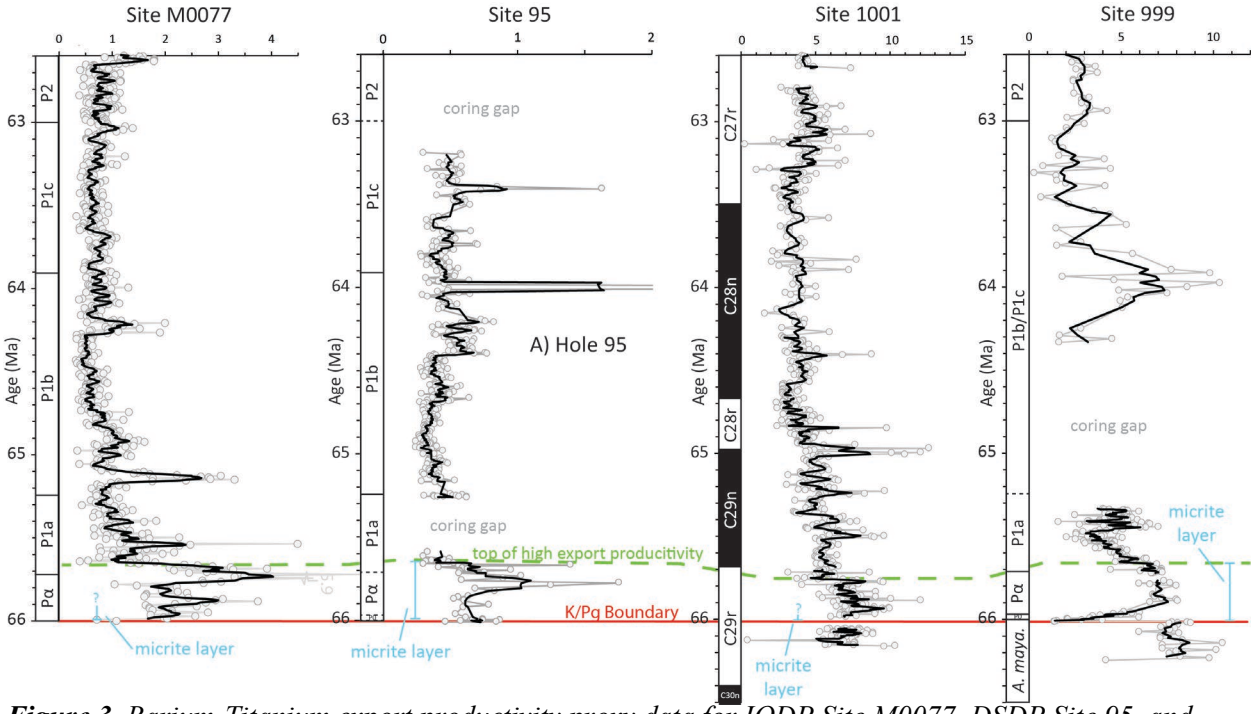

Figure 3. *Barium-Titanium export productivity proxy data for IODP Site M0077, DSDP Site 95, and ODP Sites 1001 and 999. Individual datapoints are grey circles, thick black lines is a 5-point moving average. Red line indicates the K-Pg boundary (or the top of the boundary interval in the case of Sites M0077 and 95), blue line indicates the thickness of the micrite layer identified at each site by Bralower et al. (2020), and the green dashed line indicates the top of the interval of highest export productivity at each site.*

minimum about 1.2 myr after the K-Pg boundary, at which point values stabilize and remain low with some small-scale variability. Interestingly, this transition around 1.2 myr post-impact coincides with turnover in the calcareous nannoplankton ecosystem, as disaster taxa began to give way to acmes of new Paleocene taxa (Jones et al., 2019; Lowery et al., 2021).

3.2.2 Site 95

Ba/Ti ratios at Site 95 are also highest in the earliest Paleocene, with a peak around the Pα/P1a zonal boundary and a sharp drop off ~340 kyr after the impact. A difference of 20 kyr between two sites whose age models are entirely based on biostratigraphy is basically within error and we feel comfortable assuming that this drop was contemporaneous with the one observed at Chicxulub Crater Site M0077. Approximately 300 kyr of the record in the middle of zone P1a is erased by a coring gap, but above this level Ba/Ti values trend lower until about 1.1 myr after the K-Pg boundary. Values then remain low until about 1.6 myr post-impact and then increase somewhat, varying through the rest of the record.

3.2.3 Site 1001

Site 1001 is the first site in which there are data for the latest Cretaceous, and we can see that (above a gap where the boundary layer is mostly missing) Ba/Ti values increased in the Danian relative to the Maastrichtian. Although there is no obvious peak like in the two Gulf of Mexico sites, there is still an interval of overall higher values lasting to ~ 280 kyr after the impact. Above this level, values are much more variable than in the Gulf of Mexico but there is still a clear downward trend to a nadir around 1.4 myr after the K-Pg boundary, above which point values increase slightly and vary a little bit for the rest of the record.

3.2.4 Site 999

Site 999 is the southernmost site, and the most distal from the Chicxulub impact crater. Ba/Ti values are very low directly above the boundary layer, quickly increasing through the lower part of zone Pα. Higher values after this brief recovery interval do no exceed the Ba/Ti values observed in the latest

312 Cretaceous, but they are much higher than subsequent Paleocene values (with the exception of a brief
313 peak around 2 myr after the K-Pg boundary). Once again, there is a sharp drop in values approximately
314 320 kyr post-impact followed by gradually declining values. The very poor quality of the biostratigraphy
315 in this core (the Pα/P1a zonal boundary marker is really the only reliable datum) makes it difficult to
316 determine the timing of this decline and whether the increase observed below the coring gap really occurs
317 just 600 kyr after the boundary or much later. While we do not place much confidence in the ages above
318 this level, we are confident in age control in the key interval above the boundary, specifically the highest
319 occurrence of *P. eugubina* (Pα/P1a zonal boundary).

320 **4. Discussion**

321 **4.1 Regional Homogeneity of Post K-Pg Export Production**

322 The most striking feature of the four export productivity records presented here, and the key
323 result of this investigation, is the consistent occurrence of relatively elevated Ba/Ti values in the earliest
324 Paleocene. The interval of highest export production ends right around the Pα/P1a zonal boundary at each
325 site, roughly 300 kyr after the K-Pg boundary, followed by a general decline over the next million years
326 or so. The precise features of this record vary from site to site; notably, the prominent early peak observed
327 in the Gulf of Mexico (Sites M0077 and 95) is absent in the Caribbean cores (Sites 999 and 1001).
328 Likewise, Site 999 records very low values immediately above the K-Pg boundary followed by a rapid
329 recovery of values that is not evident at any of the other sites. Finally, the timing of the sharp decline of
330 these high productivity intervals varies by a few tens of kyrs between sites. Because the age models are
331 based on biostratigraphy *or* paleomagnetic reversals, with no higher resolution techniques like orbital
332 chronology, it is impossible to say whether these differences are real or merely artifacts of the limits of
333 the age model. These are superficial differences, though, and a clear overall trend exists that export
334 productivity was very elevated across Gulf of Mexico and Caribbean (a distance of ~1700 km) for ~300
335 kyr after the K-Pg mass extinction, and began to decline thereafter.

The observed homogeneity in regional export productivity in the earliest Paleocene provides important context for previous observations of global-scale heterogeneity. That work had shown major differences in export productivity between ocean basins, with an increase in export production observed in the Central Pacific, a decline in the North Atlantic and northern South Atlantic, and no change in the southern South Atlantic (Hull and Norris, 2011). Those sites are widely separated and all represent different oceanographic environments (oligotrophic tropical gyres, western boundary currents, eastern boundary currents). With only one site in each region, it is hard to know how much confidence to put into these regional trends. With the discovery that sites within the Gulf of Mexico/Caribbean all exhibit the same trends, we can be more confident that previously observed regional differences are real. Whatever the processes controlling these differences in post-extinction export productivity they are operating over a relatively wide area. Armed with this knowledge, we can better evaluate possible drivers of globally heterogeneous export productivity in the post-extinction ocean.

4.2 Drivers of Post-Extinction Export Productivity

The second-most striking feature of our data is that at two of our sites (Site 95 and 999) the interval of high export productivity ~300 kyr after the boundary coincides almost exactly with well-defined intervals microcrystalline calcite ("micrite") identified by Bralower et al. (2020). The widespread deposition of micrite in marine settings after the K-Pg boundary was documented by Bralower et al. (2020), and proposed to be primarily formed by microbial blooms. The structure of individual micrite crystals is similar to that produced by various cyanobacteria (Bralower et al., 2020) and the micrite layer itself at several sites is associated with elevated biomarkers for photosynthetic bacteria and eukaryotic algae (Sepúlveda et al., 2009; Schaefer et al., 2020; Bralower et al., 2020). Some portion of the global micrite layer was also likely formed by the backreaction of CaO or CaOH vaporized by the Chicxulub impact, but this process would have been limited to the years after the impact as ejecta fell out of the atmosphere (Bralower et al., 2020) and wouldn't explain micrite deposition over ~300 kyr.

Extensive recrystallization of carbonate material at Sites M0077 obscures the micrite record at those locations. At Site M0077, abundant micrite is limited to a zone of good preservation which includes the "Transitional Unit" at the top of the K-Pg boundary layer (Morgan et al., 2017) and an overlying layer of green marlstone dated to the base of planktic foraminifer zone Pα (Bralower et al., 2020). Above this in the overlying white limestone layer, poor preservation prevents the consistent identification of micrite. At Site 1001, coring gaps in the boundary interval in Hole 1001B limit the identification of the micrite layer to a minimum thickness (17 cm, Bralower et al., 2020). Thus, we have two sites showing a clear deposition of micrite until it ends at the same stratigraphic position (Sites 95 and 999), and two other sites with insufficient data to say one way or the other (Sites M0077 and 1001).

Three other open ocean sites have evidence of increased export productivity in the earliest Danian: the tropical Pacific Shatsky Rise and Hess Rise (Alegret and Thomas, 2005, 2009; Hull and Norris, 2011), and the mid-latitude South Pacific sections around Marlborough, South Island, New Zealand (Hollis et al., 1995, 2003). The high export productivity at Marlborough appears to be the result of increased upwelling along an upwelling-prone continental margin (Hollis et al., 2003). Shatsky Rise and Hess Rise, though, are open ocean sites on roughly the same paleolatitude as our study area and are generally oligotrophic during this time interval (e.g., Deprez et al., 2017). Unfortunately, no sites at these locations have both Ba/Ti data and micrite data. Micrite is enriched at Shatsky Rise Site 1209 over a 6 cm interval above the boundary, and at 1210 over a 7 cm interval above the boundary (Bralower et al., 2020). At Hess Rise Site 465, micrite is enriched over a 24 cm interval above the boundary. Unfortunately, overall low Ti abundance at Site 1209 results in low-confidence Ba/Ti data, while Ba/Fe data don't reveal much change at all across the K-Pg boundary (Hull and Norris, 2011). No elemental data exist for Site 1210, but at nearby Site 577, barium proxies indicate a ~100 kyr interval of increased export production (Hull and Norris, 2011).

Benthic foraminiferal accumulation rate and assemblages provide additional export productivity information at these sites. At Site 1210, benthic foraminiferal proxies indicate increased export

productivity peaking just after the boundary and remaining elevated for ~ 100 kyr (Alegret and Thomas, 2009). This peak in export productivity occurs within the 7 cm thick micrite layer (Bralower et al., 2020), and the subsequent sharp decline in export production occurs above the micrite layer. Likewise, at Site 465 on Hess Rise, benthic foraminifer data indicate a peak in post K-Pg export production within 100 kyr of the boundary (within planktic foraminifer zone Pα) (Alegret and Thomas, 2005), right in the middle of the 24 cm thick zone of micrite enrichment (Bralower et al., 2020). It is important to point out that foraminifer samples at both sites were taken at a 10 cm resolution (Alegret and Thomas, 2005, 2009) so a precise tie between the decline in export productivity and the end of micrite deposition is impossible to make with existing data.

Given these observations, we feel confident in concluding that: 1) tropical open ocean sites were prone to increased export production immediately after the K-Pg boundary; and 2) a relationship exists between elevated export productivity and the micrite layer described by Bralower et al. (2020). Although various types of "ballast," including calcite plankton shells, have been thought to influence export production in the modern ocean (Amrstrong et al., 2001; Francois et al., 2002), it does not seem likely that micrite itself, or more specifically the cyanobacteria that produced it, is the cause of increased export production in the earliest Paleocene. Micrite is abundant at many sites which did not experience elevated export production after the K-Pg. For example, Blake Nose Site 1049, which experienced either a decline or no change in export production after the boundary (Hull and Norris, 2011), has a 30 cm thick micrite layer. Walvis Ridge Site 1267, which similarly experienced no change in post-extinction export production based on barium isotopes (Hull and Norris, 2011), has a 1.82 m thick micrite layer. All told, Bralower et al. (2020) identified micrite layers at 31 sites globally; of these, only 5 record elevated export production in the early Danian based on available proxies. All of these sites are in tropical open ocean settings which are predisposed to oligotrophy.

To explain increased export production in the Chicxulub Crater after the impact event, Lowery et al (2021) suggested that a switch in the dominant primary producers, from larger calcareous

nannoplankton to smaller picoplankton like cyanobacteria, would have increased the recycling of nutrients in the euphotic zone in an otherwise oligotrophic water column and facilitated a weaker but more efficient biological pump. The consistent observation reported here of increased post K-Pg export production at low latitude oligotrophic sites supports that explanation.

The biological pump is commonly conceptualized as having two parts: the export of some portion of net primary production (NPP) out of the euphotic zone, often referred to as pump "strength," and the sinking of that organic matter through intermediate depths to the ocean's interior (commonly defined as > 1000 m water depth), where it is considered to be removed from the short term carbon cycle, often referred to as pump "efficiency" (see Hilting et al., 2008 and review in Zhang et al., 2018). A switch from calcareous nannoplankton, the dominant phytoplankton of the Cretaceous (Bown, 2005) to smaller phytoplankton like cyanobacteria and chlorophyte algae would reduce the strength of the biological pump, because smaller cell sizes sink more slowly and are less likely to be consumed by zooplankton and packaged in fecal pellets, or bunch together in aggregates (Legrendre and Michaud, 1998; de la Rocha and Passow, 2007). Counterintuitively, though, this can make the biological pump more efficient: as more organic matter is remineralized by microbes in the euphotic zone (the "microbial loop"), the only carbon that manages to sink out of the euphotic zone is highly refractory and difficult to metabolize (Legrendre and Michaud, 1998; de la Rocha and Passow, 2007). This refractory organic matter is less likely to be remineralized by grazers as it sinks through intermediate depths, so even though a lower proportion of overall NPP sinks out of the euphotic zone (the pump is *weaker*), a larger proportion of the organic matter that exits the euphotic zones manages to sink to intermediate depths, or all the way to the seafloor (the pump is *more efficient*). In most circumstances this change results in lower overall export production, but in oligotrophic regions this change in efficiency can actually cause an increase in export production, as described by Henehan et al. (2019). The general association of the micrite layer (indicating dominance of microbial primary producers) with the elevated post-impact export production observed across Pacific and Caribbean/Gulf of Mexico sites described here suggests that a post-extinction dominance of

picophytoplankton is the primary mechanism driving elevated export productivity at previously oligotrophic parts of the open ocean in the earliest Paleocene.

While it appears that the dominance of picophytoplankton is the proximal cause of elevated post K-Pg export production in tropical open ocean waters, it is important to note that the timing is different between the Caribbean and the central Pacific. The period of highest export production drops off ~ 300 kyr after the K-Pg in the Gulf of Mexico and Caribbean but ends much earlier at Shatsky and Hess Rises, after ~ 100 kyr (Alegret and Thomas, 2005, 2009; Hull and Norris, 2011). This is in line with previous results which indicate a global diachroneity in the turnover of calcareous nannoplankton assemblages in the earliest Paleocene (Jones et al., 2019), driven by transition from surface waters characterized by efficient recycling of nutrients due to the prevalence of picophytoplankton feeding the microbial loop, to surface waters characterized by less efficient recycling of nutrients caused by greater export of larger plankton out of the euphotic zone (Jones et al., 2019; Lowery et al., 2021). At Shatsky Rise, disaster assemblages of calcareous nannoplankton gave way to acmes of Paleocene taxa soon after the K-Pg (Alvarez et al., 2019; Jones et al., 2019). On the other hand, disaster taxa in the Chicxulub Crater continue until the final decline in export productivity about a million years after the K-Pg (Jones et al., 2019), and at Site 999, disaster taxa continue at least into zone P1a >300 kyr after the K-Pg (Sigurdsson et al., 1997). Whether the recovery in calcareous nannoplankton caused the observed change in export production or if a reduction in export production spurred the local diversification of calcareous nannoplankton remains an open question.

Conclusions

Our new XRF-derived Ba/Ti export productivity proxy data from the Gulf of Mexico and Caribbean show a post K-Pg peak in export productivity across the region, with an interval of high values lasting for ~ 300 kyr after the boundary and then declining values for another ~ 700 kyr. This is a major improvement on previous compilations of earliest Paleocene export productivity, which showed that post-extinction changes in export production were globally heterogeneous but only on an ocean basin scale.

Our results show that broad regions followed similar trends. In particular, we find that most elevated export production in the earliest Danian is found at tropical open ocean sites (Shatsky Rise, Hess Rise, and our Caribbean/Gulf of Mexico sites) typically pre-disposed to oligotrophy.

Our other major observation is that at sites with elevated export production and at which preservation makes such observations possible, the post K-Pg global micrite layer corresponds with the interval of elevated export production. We interpret this as evidence that the dominance of picophytoplankton like cyanobacteria and chlorophyte algae associated with the micrite deposition (Bralower et al., 2020) altered the dynamics of the biological pump to increase recycling of organic matter in the euphotic zone. Enhanced recycling of organic matter left only refractory organic matter, which is more difficult to recycle, to be exported from the euphotic zone; because it is refractory it would have been more likely to sink through the water column than more labile organic matter exported under normal conditions. In typically oligotrophic environments, this slight increase in efficiency of the biologic pump could have resulted in overall higher export production; as larger phytoplankton recovered and more labile organic matter was exported and grazed, enhanced export production would have subsided.

More datasets from a wider range of latitudes and ocean basins are needed to build a more complete picture of post K-Pg export production to more fully understand how the marine biosphere recovered from the most recent major mass extinction.

Data Availability Statement

XRF core scan data and age models are archived at the NCEI Paleoclimate Database here: https://www.ncei.noaa.gov/access/paleo-search/study/35081

Acknowledgements

We are grateful to Brian LeVay and Mackenzie Schoemann of the IODP Gulf Coast Repository (GCR) at Texas A&M University for their assistance with XRF core scanning, the staff of the GCR for sending samples from Sites 95 and 536 for biostratigraphic analysis, and Vinny Percuoco at the GCR for providing high resolution photograph for the K-Pg boundary in Hole 1001B. We are also grateful to Ryan Weber and Calvin Gordon of PaleoData, Inc., for their assistance preparing samples from Site 999 and 1001 for biostratigraphic analysis.

Figure 1. Map showing position of our study sites around the time of the K-Pg Boundary. Map modified after Pindell and Barrett (1990) and Snedden et al. (2021).

Figure 2. Stratigraphic sections showing lithostratigraphy, core scan photographs, and images of the K-Pg boundary of the studied intervals from DSDP Hole 95, ODP Hole 1001A, and ODP Hole 999B. Lithostratigraphy follows shipboard descriptions Worzel, Bryant et al. (1973) for Site 95 and Sigurdsson et al., 1997 for Sites 999 and 1001). Core scan photographs were collected at the GCR at the same time XRF data were collected (except for the photograph of the K-Pg boundary in Hole 1001B, which is from the ODP photo archives). Mbsf = meters below sea floor, PFZ = Planktic Foraminifer Zone, Lith. = lithology, PMag = Paleomagnetic polarity, E. Campanian = Early Campanian, Maas. = Maastrichtian, *G. elevata* = *Globotruncanita elevate, A.m.* and *A. mayaroensis* = *Abathomphalus mayaroensis*.

Figure 3. Barium-Titanium export productivity proxy data for IODP Site M0077, DSDP Site 95, and ODP Sites 1001 and 999. Individual datapoints are grey circles, thick black lines is a 5-point moving average. Red line indicates the K-Pg boundary (or the top of the boundary interval in the case of Sites M0077 and 95), blue line indicates the thickness of the micrite layer identified at each site by Bralower et al. (2020), and the green dashed line indicates the top of the interval of highest export productivity at each site.

References

505 Alegret, L., & Thomas, E. (2005). Cretaceous/Paleogene boundary bathyal paleo-environments in the
506 central North Pacific (DSDP Site 465), the Northwestern Atlantic (ODP Site 1049), the Gulf of
507 Mexico and the Tethys: The benthic foraminiferal record. Palaeogeography, Palaeoclimatology,
508 Palaeoecology, 224(1-3), 53-82.

509 Alegret, L., & Thomas, E. (2007). Deep-sea environments across the Cretaceous/Paleogene boundary in
510 the eastern South Atlantic Ocean (ODP leg 208, Walvis Ridge). Marine Micropaleontology, 64(1-
511 2), 1-17.

512 Alegret, L., & Thomas, E. (2009). Food supply to the seafloor in the Pacific Ocean after the
513 Cretaceous/Paleogene boundary event. Marine Micropaleontology, 73(1-2), 105-116.

514 Alegret, L., Thomas, E., & Lohmann, K. C. (2012). End-Cretaceous marine mass extinction not caused by
515 productivity collapse. Proceedings of the National Academy of Sciences, 109(3), 728-732.

516 Armstrong, R. A., Lee, C., Hedges, J. I., Honjo, S., & Wakeham, S. G. (2001). A new, mechanistic model
517 for organic carbon fluxes in the ocean based on the quantitative association of POC with ballast
518 minerals. Deep Sea Research Part II: Topical Studies in Oceanography, 49(1-3), 219-236.

519 Artemieva, N., Morgan, J., & Expedition 364 Science Party. (2017). Quantifying the release of climate-
520 active gases by large meteorite impacts with a case study of Chicxulub. Geophysical Research
521 Letters, 44(20), 10-180.

522 Artemieva, N., & Morgan, J. (2020). Global K-Pg layer deposited from a dust cloud. Geophysical
523 Research Letters, 47(6), e2019GL086562.

524 Bains, S., Norris, R. D., Corfield, R. M., & Faul, K. L. (2000). Termination of global warmth at the
525 Palaeocene/Eocene boundary through productivity feedback. Nature, 407(6801), 171-174.

526 Bardeen, C. G., Garcia, R. R., Toon, O. B., & Conley, A. J. (2017). On transient climate change at the
527 Cretaceous− Paleogene boundary due to atmospheric soot injections. Proceedings of the National
528 Academy of Sciences, 114(36), E7415-E7424.

529 Barton, A. D., Irwin, A. J., Finkel, Z. V., & Stock, C. A. (2016). Anthropogenic climate change drives
530 shift and shuffle in North Atlantic phytoplankton communities. Proceedings of the National
531 Academy of Sciences, 113(11), 2964-2969.

532 Berggren, W. A., & Pearson, P. N. (2005). A revised tropical to subtropical Paleogene planktonic
533 foraminiferal zonation. The Journal of Foraminiferal Research, 35(4), 279-298.

534 Birch, H. S., Coxall, H. K., Pearson, P. N., Kroon, D., & Schmidt, D. N. (2016). Partial collapse of the
535 marine carbon pump after the Cretaceous-Paleogene boundary. Geology, 44(4), 287-290.

536 Birch, H., Schmidt, D. N., Coxall, H. K., Kroon, D., & Ridgwell, A. (2021). Ecosystem function after the
537 K/Pg extinction: decoupling of marine carbon pump and diversity. Proceedings of the Royal
538 Society B, 288(1953), 20210863.

539 Bown, P. (2005). Selective calcareous nannoplankton survivorship at the Cretaceous-Tertiary boundary.
540 Geology, 33(8), 653-656.

541 Boyd, P., & Newton, P. (1995). Evidence of the potential influence of planktonic community structure on
542 the interannual variability of particulate organic carbon flux. Deep Sea Research Part I:
543 Oceanographic Research Papers, 42(5), 619-639.

544 Boyd, P. W., & Trull, T. W. (2007). Understanding the export of biogenic particles in oceanic waters: Is
545 there consensus?. Progress in Oceanography, 72(4), 276-312.

546 Bralower, T. J., Paull, C. K., & Mark Leckie, R. (1998). The Cretaceous-Tertiary boundary cocktail:
547 Chicxulub impact triggers margin collapse and extensive sediment gravity flows. Geology, 26(4),
548 331-334.

549 Bralower, T. J., Cosmidis, J., Heaney, P. J., Kump, L. R., Morgan, J. V., Harper, D. T., ... & Vajda, V.
550 (2020). Origin of a global carbonate layer deposited in the aftermath of the Cretaceous-Paleogene
551 boundary impact. Earth and Planetary Science Letters, 548, 116476.

552 Buesseler, K. O. (1998). The decoupling of production and particulate export in the surface ocean. Global
553 Biogeochemical Cycles, 12(2), 297-310.

554 Buesseler, K. O., & Boyd, P. W. (2009). Shedding light on processes that control particle export and flux
555 attenuation in the twilight zone of the open ocean. Limnology and Oceanography, 54(4), 1210-
556 1232.

557 Buffler, R.T., Schlager, W., et al. (1984). Initial Reports of the Deep Sea Drilling Project 77,
558 doi:10.2973/dsdp.proc.77.1984

559 Coxall, H. K., D'Hondt, S., & Zachos, J. C. (2006). Pelagic evolution and environmental recovery after
560 the Cretaceous-Paleogene mass extinction. Geology, 34(4), 297-300.

561 Culver, S. J. (2003). Benthic foraminifera across the Cretaceous–Tertiary (K–T) boundary: a review.
562 Marine Micropaleontology, 47(3-4), 177-226.

563 D'Hondt, S., Donaghay, P., Zachos, J. C., Luttenberg, D., & Lindinger, M. (1998). Organic carbon fluxes
564 and ecological recovery from the Cretaceous-Tertiary mass extinction. Science, 282(5387), 276-
565 279.

566 De La Rocha, C. L., & Passow, U. (2007). Factors influencing the sinking of POC and the efficiency of
567 the biological carbon pump. Deep Res II 54: 639–658.

568 Deprez, A., Jehle, S., Bornemann, A., & Speijer, R. P. (2017). Pronounced biotic and environmental
569 change across the latest Danian warming event (LDE) at Shatsky Rise, Pacific Ocean (ODP Site
570 1210). *Marine Micropaleontology*, *137*, 31-45.

571 Denne, R. A., Scott, E. D., Eickhoff, D. P., Kaiser, J. S., Hill, R. J., & Spaw, J. M. (2013). Massive
572 Cretaceous-Paleogene boundary deposit, deep-water Gulf of Mexico: New evidence for
573 widespread Chicxulub-induced slope failure. Geology, 41(9), 983-986.

574 Doyle, P. S., & Riedel, W. R. (1979). Ichthyoliths: present status of taxonomy and stratigraphy of
575 microscopic fish skeletal debris. Scripps Institution of Oceanography, University of California at
576 San Diego.

577 Dymond, J., Suess, E., & Lyle, M. (1992). Barium in deep-sea sediment: A geochemical proxy for
578 paleoproductivity. Paleoceanography, 7(2), 163-181.

579 Eagle, M., Paytan, A., Arrigo, K. R., van Dijken, G., & Murray, R. W. (2003). A comparison between
580 excess barium and barite as indicators of carbon export. Paleoceanography, 18(1).

581 Esmeray-Senlet, S., Wright, J. D., Olsson, R. K., Miller, K. G., Browning, J. V., & Quan, T. M. (2015).
582 Evidence for reduced export productivity following the Cretaceous/Paleogene mass extinction.
583 Paleoceanography, 30(6), 718-738.

584 Fraass, A. J., Kelly, D. C., & Peters, S. E. (2015). Macroevolutionary history of the planktic foraminifera.
585 Annual Review of Earth and Planetary Sciences, 43, 139-166.

586 Francois, R., Honjo, S., Manganini, S. J., & Ravizza, G. E. (1995). Biogenic barium fluxes to the deep
587 sea: Implications for paleoproductivity reconstruction. Global Biogeochemical Cycles, 9(2), 289-
588 303.

589 Francois, R., Honjo, S., Krishfield, R., & Manganini, S. (2002). Factors controlling the flux of organic
590 carbon to the bathypelagic zone of the ocean. Global Biogeochemical Cycles, 16(4), 34-1.

591 Gibbs, S. J., Bown, P. R., Ward, B. A., Alvarez, S. A., Kim, H., Archontikis, O. A., Sauterey, B. Poulton, A.
592 J., Wilson, J., & Ridgwell, A. (2020). Algal plankton turn to hunting to survive and recover from
593 end-Cretaceous impact darkness. *Science advances*, *6*(44), eabc9123.

Gradstein, F. M., Ogg, J. G., Schmitz, M. D., & Ogg, G. M. (Eds.). (2012). The geologic time scale 2012. elsevier.

Griffith, E. M., & Paytan, A. (2012). Barite in the ocean–occurrence, geochemistry and palaeoceanographic applications. Sedimentology, 59(6), 1817-1835.

Hallock, P. (1987). Fluctuations in the trophic resource continuum: a factor in global diversity cycles?. Paleoceanography, 2(5), 457-471.

Henehan, M. J., Ridgwell, A., Thomas, E., Zhang, S., Alegret, L., Schmidt, D. N., Rae, J. W. B., Witts, J. D., Landman, N. H., Greene, S. E., & Hull, P. M. (2019). Rapid ocean acidification and protracted Earth system recovery followed the end-Cretaceous Chicxulub impact. Proceedings of the National Academy of Sciences, 116(45), 22500-22504.

Henson, S. A., Sanders, R., & Madsen, E. (2012). Global patterns in efficiency of particulate organic carbon export and transfer to the deep ocean. Global Biogeochemical Cycles, 26(1).

Hollis, C. J., Rodgers, K. A., & Parker, R. J. (1995). Siliceous plankton bloom in the earliest Tertiary of Marlborough, New Zealand. Geology, 23(9), 835-838.

Hollis, C. J., Strong, C. P., Rodgers, K. A., & Rogers, K. M. (2003). Paleoenvironmental changes across the Cretaceous/Tertiary boundary at Flaxbourne River and Woodside Creek, eastern Marlborough, New Zealand. New Zealand Journal of Geology and Geophysics, 46(2), 177-197.

Hsü, K. J., & Mckenzie, J. A. (1985). A “Strangelove” ocean in the earliest Tertiary. The Carbon Cycle and Atmospheric CO2: Natural Variations Archean to Present, 32, 487-492.

Hull, P. M., & Norris, R. D. (2011). Diverse patterns of ocean export productivity change across the Cretaceous-Paleogene boundary: New insights from biogenic barium. Paleoceanography, 26(3).

615 Jiang, S., Bralower, T. J., Patzkowsky, M. E., Kump, L. R., & Schueth, J. D. (2010). Geographic controls
616 on nannoplankton extinction across the Cretaceous/Palaeogene boundary. Nature Geoscience,
617 3(4), 280-285.

618 Jones, H. L., Lowery, C. M., & Bralower, T. J. (2019). Delayed calcareous nannoplankton boom-bust
619 successions in the earliest Paleocene Chicxulub (Mexico) impact crater. Geology, 47(8), 753-756.

620 Thierstein, H. R. (1982). Terminal Cretaceous plankton extinctions: A critical assessment. Geological
621 implications of impacts of large asteroids and comets on the earth, 190, 385-399.

622 Legendre, L., & Michaud, J. (1998). Flux of biogenic carbon in oceans: size-dependent regulation by
623 pelagic food webs. *Marine Ecology Progress Series*, *164*, 1-11.

624 Legendre, L., & Rivkin, R. B. (2002). Fluxes of carbon in the upper ocean: regulation by food-web
625 control nodes. Marine Ecology Progress Series, 242, 95-109.

626 Louvel, V., & Galbrun, B. (2000). Magnetic polarity sequences from downhole measurements in ODP
627 holes 998B and 1001A, leg 165, Caribbean Sea. Marine Geophysical Researches, 21(6), 561-577.

628 Lowery, C. M., Bralower, T. J., Owens, J. D., Rodríguez-Tovar, F. J., Jones, H., Smit, J., Whalen, M. T.,
629 Claeys, P., Farley, K., Gulick, S. P. S., Morgan, J. V., Green, S., Chenot, E., Christeson, G. L.,
630 Cockell, C. S. Coolen, M. J. L., Ferrière, L., Gebhardt, C., Goto, K., Kring, D. A., Lofi, J.,
631 Ocampo-Torres, R., Perez-Cruz, L., Pickersgill, A. E., Poelchau, M. H., Rae, A. S. P., Rasmussen
632 C., Rebolledo-Vieyra, M., Riller, U., Sato, H., Tikoo, S. M., Tomioka, N., Urrutia-Fucugauchi, J.,
633 Vellekoop, J., Wittmann, A., Xiao, L., Yamaguchi, K. E., & Zylberman, W. (2018). Rapid
634 recovery of life at ground zero of the end-Cretaceous mass extinction. Nature, 558(7709), 288-
635 291.

636 Lowery, C. M., Bown, P. R., Fraass, A. J., & Hull, P. M. (2020). Ecological response of plankton to
637 environmental change: thresholds for extinction. Annual Review of Earth and Planetary Sciences,
638 48, 403-429.

639 Lowery, C. M., Jones, H., Bralower, T. J., Perez Cruz, L., Gebhardt, C., Whalen, M. T., Chenot, E., Smit,
640 J., Purkey Phillips, M., Choumiline, K., Arenillas, I., Arz, J. A., Garcia, F., Ferrand, M., Gulick,
641 S. P. S., and IODP Expedition 364 Scientists. (2021) Early Paleocene paleoceanography and
642 export productivity in the Chicxulub crater. Paleoceanography & Paleoclimatology.

643 Molina, E., Alegret, L., Arenillas, I., Arz, J. A., Gallala, N., Hardenbol, J., von Salis, K., Steurbaut, E.,
644 Vandenberghe, N., & Zaghbib-Turki, D. (2006). The global boundary stratotype section and point
645 for the base of the Danian stage (Paleocene, Paleogene," Tertiary", Cenozoic) at El Kef, Tunisia-
646 original definition and revision. Episodes, 29(4), 263.

647 Morgan, J., Gulick, S., Mellett, C. L., & Green, S. L. (2017). Chicxulub: drilling the K-Pg impact crater.
648 Proceedings of the International Ocean Discovery Program, 364.
649 https://doi.org/10.14379/iodp.proc.364.2017

650 Müller, P. J. and Suess, E., 1979. Productivity, sedimentation rate, and sedimentary organic matter in the
651 oceans—I. Organic carbon preservation. Deep Sea Research Part A. Oceanographic Research
652 Papers, 26(12), pp.1347-1362.

653 Olsson, R. K., Berggren, W. A., Hemleben, C., & Huber, B. T. (1999). Atlas of Paleocene planktonic
654 foraminifera. Smithsonian Contributions to Paleobiology 85, 1-106

655 Paytan, A., Kastner, M., & Chavez, F. P. (1996). Glacial to interglacial fluctuations in productivity in the
656 equatorial Pacific as indicated by marine barite. Science, 274(5291), 1355-1357.

657 Paytan, A., & Griffith, E. M. (2007). Marine barite: Recorder of variations in ocean export productivity.
658 Deep Sea Research Part II: Topical Studies in Oceanography, 54(5-7), 687-705.

Pindell, J. L., & Barrett, S. F. (1990). Caribbean plate tectonic history. *The Caribbean Region, volume H of The Geology of North America*, 405-432.

Sanford, J. C., Snedden, J. W., & Gulick, S. P. (2016). The Cretaceous-Paleogene boundary deposit in the Gulf of Mexico: Large-scale oceanic basin response to the Chicxulub impact. Journal of Geophysical Research: Solid Earth, 121(3), 1240-1261.

Schaefer, B., Grice, K., Coolen, M. J., Summons, R. E., Cui, X., Bauersachs, T., Böttcher, M.E., Bralower, T.J., Lyons, S.L. and Freeman, K.H, Cockell, C. S., Gulick, S. P. S., Morgan, J. V., Whalen, M. T., Lowery, C. M., & Vajda, V. (2020). Microbial life in the nascent Chicxulub crater. Geology, 48(4), 328-332.

Schueth, J. D., Bralower, T. J., Jiang, S., & Patzkowsky, M. E. (2015). The role of regional survivor incumbency in the evolutionary recovery of calcareous nannoplankton from the Cretaceous/Paleogene (K/Pg) mass extinction. Paleobiology, 41(4), 661-679.

Sepúlveda, J., Wendler, J. E., Summons, R. E., & Hinrichs, K. U. (2009). Rapid resurgence of marine productivity after the Cretaceous-Paleogene mass extinction. Science, 326(5949), 129-132.

Sepúlveda, J., Alegret, L., Thomas, E., Haddad, E., Cao, C., & Summons, R. E. (2019). Stable isotope constraints on marine productivity across the Cretaceous-Paleogene mass extinction. Paleoceanography and Paleoclimatology, 34(7), 1195-1217.

Sibert, E. C., & Norris, R. D. (2015). New Age of Fishes initiated by the Cretaceous− Paleogene mass extinction. Proceedings of the National Academy of Sciences, 112(28), 8537-8542.

Sigurdsson, H., Leckie, R.M., Acton, G.D., et al., 1997. Proceedings of the Ocean Drilling Program, Initial Reports., 165: College Station, TX (Ocean Drilling Program). doi:10.2973/odp.proc.ir.165.1997

681 Snedden, J., Leshyk, V. O., and Kring, D. (2021). Paleogeographic Evolution of the Chicxulub Region.
682 Lunar and Planetary Institute illustration,
683 https://www.lpi.usra.edu/exploration/training/illustrations/chicxulub-effects/, accessed 9/27/21.

684 Thierstein, H. R. (1982). Terminal Cretaceous plankton extinctions: A critical assessment. Geological
685 implications of impacts of large asteroids and comets on the earth, 190, 385-399.

686 Toon, O. B., Zahnle, K., Morrison, D., Turco, R. P., & Covey, C. (1997). Environmental perturbations
687 caused by the impacts of asteroids and comets. Reviews of Geophysics, 35(1), 41-78.

688 Wade, B. S., Pearson, P. N., Berggren, W. A., & Pälike, H. (2011). Review and revision of Cenozoic
689 tropical planktonic foraminiferal biostratigraphy and calibration to the geomagnetic polarity and
690 astronomical time scale. Earth-Science Reviews, 104(1-3), 111-142.

691 Worzel, J. L., Bryant, W., et al, 1973, Initial Reports of the Deep Sea Drilling Project, Volume X,
692 Washington (U.S. Government Printing Office) doi:10.2973/dsdp.proc.10.1973

693 Zachos, J. C., & Arthur, M. A. (1986). Paleoceanography of the Cretaceous/Tertiary boundary event:
694 inferences from stable isotopic and other data. Paleoceanography, 1(1), 5-26.

695 Zachos, J. C., Arthur, M. A., & Dean, W. E. (1989). Geochemical evidence for suppression of pelagic
696 marine productivity at the Cretaceous/Tertiary boundary. Nature, 337(6202), 61-64.

697 Zhang, C., Dang, H., Azam, F., Benner, R., Legendre, L., Passow, U., Polimene, L., Robinson, C., Suttle,
698 C. A., & Jiao, N. (2018). Evolving paradigms in biological carbon cycling in the ocean. National
699 Science Review, 5(4), 481-499.